THESIS FOR THE DEGREE OF LICENTIATE OF ENGINEERING

Synthesis of tailored nanoparticles for supported oxidation catalysts

Yanyue Feng

Department of Chemistry and Chemical Engineering
CHALMERS UNIVERSITY OF TECHNOLOGY

Göteborg, Sweden 2022

Synthesis of tailored nanoparticles for supported oxidation catalysts
YANYUE FENG

Licentiatuppsatser vid institutionen för kemi och kemiteknik
Chalmers tekniska högskola
Nr 2022:03

Department of Chemistry and Chemical Engineering
Chalmers University of Technology
SE-412 96 Göteborg
Sweden
Telephone: +46 (0)767084885

Printed by Chalmers Reproservice
Göteborg, Sweden 2022

Synthesis of tailored nanoparticles for supported oxidation catalysts
Thesis for the degree of Licentiate of Engineering
YANYUE FENG

Department of Chemistry and Chemical Engineering
Chalmers University of Technology

Abstract

The transition from microscale to nanoscale materials design leads to immense changes of physical and chemical properties of the materials. For decades, the design and making of functional nanomaterials have been at the frontier of what can be achieved, even with the more sophisticated synthesis methods. Thanks to the recent rapid development of synthesis and characterization techniques, multicomponent nanoparticle catalysts are gaining more and more interest because they can be tailored to exhibit higher catalytic efficiency than their monocomponent counterparts. Among them, Au and Pd based catalysts with core@shell structure has attracted great attention due to the possibilities of tuning the catalytic activity by the utilization of unique surface properties such as strain.

In this study, Au@Pd core@shell nanoparticles were synthesized by a two-steps seeded growth method. The effects of different synthesis parameters, including temperature and Au/Pd molar ratio, on the size of Au@Pd core@shell nanoparticles were investigated. The morphology of the as prepared Au@Pd and Au@Pd/γ-Al_2O_3 core@shell nanoparticles was imaged by high resolution transmission electron microscopy (HRTEM) and high-angle annular dark-field scanning transmission electron microscopy (HAADF - STEM). It is shown that Au@Pd core@shell nanoparticles with thin Pd shell can be successfully synthesized and loaded onto alumina using precise synthesis conditions. Moreover, neither agglomeration nor destruction of the core@shell motif under CO oxidation reaction conditions could be observed, indicating good structural stability. Further, *in situ* infrared spectroscopy reveals that palladium surface properties differ compared to palladium only particles suggesting electronic and structural modification of the Pd shell surface by the Au core.

Keywords: Supported core@shell nanoparticles, structural stability, CO oxidation

List of Publications

This thesis is based on the following appended papers

Paper I:
Synthesis and stability of supported Au core - Pd shell nanoparticles with thin shell thickness
Yanyue Feng, Andreas Schaefer, Mengqiao Di, Mattias Bauer and Per-Anders Carlsson
Manuscript

Paper II:
Chasing PtO_x species in ceria supported platinum during CO oxidation extinction with correlative *operando* spectroscopic techniques
Mengqiao Di, Kerry Simmance, Andreas Schaefer, Yanyue Feng, Felix Hemmingsson, Magnus Skoglundh, Tamsin Bell, David Thompsett, Lucy Idowu Ajakaiye Hensen, Sara Blomberg and Per-Anders Carlsson
Submitted

My Contribution

Paper I:
Main author. Responsible for synthesis and characterization of the core-shell nanoparticles and catalyst, activity and stability test, and for writing the first draft of the manuscript.

Paper II:
Co-author. Responsible for TEM imaging and EDS mapping.

List of Figures

3.1 Graphical description of synthesis of Au@Pd/Al_2O_3 nanoparticles. . . 10

4.1 TEM images of Au@Pd nanoparticles synthesized under different temperatures (a) 1 °C (b) 20 °C (c) 80 °C. 13
4.2 TEM images of Au@Pd core@shell nanoparticles with different Au/Pd molar ratios (a) 0.32 (b) 0.032 and (c) 0.0032. 15
4.3 DRIFTS spectra of CO adsorption experiment over (a) Au@Pd/Al_2O_3 nanoparticle catalyst. (b) Pd/Al_2O_3 nanoparticle catalyst. 16
4.4 TEM images and EDS linescan profiles of Au@Pd/Al_2O_3 before and after CO oxidation 17
4.5 DRIFTS spectra of CO oxidation (extinction) over (a)Pd/Al_2O_3 from 198 °C to 33 °C; (b)Pt/Al_2O_3 from 211 °C to 34 °C; (c) Au@Pd/Al_2O_3. 18

Notation

DRIFTS Diffuse reflectance infrared fourier transform spectroscopy.

EDS energy-dispersive X-ray spectroscopy.

HAADF-STEM high angle annular dark field scanning transmission electron microscopy.

HRTEM high resolution transmission electron microscopy.

MSI metal support interaction.

TEM transmission electron microscopy.

XRD X-ray diffraction.

Contents

Abstract iii

List of Publications v

List of Figures vii

Notation ix

Contents xi

1 Introduction 1
1.1 Objective 2

2 Background 3
2.1 Supported monometallic catalysts 3
2.1.1 Promotion by active supports 3
2.2 Supported bimetallic catalysts 4
2.2.1 Alloyed nanoparticles 5
2.2.2 Core-shell nanoparticles 5
2.3 Synthesis of core@shell nanoparticles 6

3 Methodology 9
3.1 Synthesis 9
3.1.1 Au@Pd core@shell nanoparticles and Au@Pd/Al_2O_3 nanoparticle catalyst 9
3.2 Characterization 10
3.2.1 Transmission Electron Microscopy (TEM) and High Resolution Transmission Electron Microscopy (HRTEM) . . 10
3.2.2 X-ray Diffraction (XRD) 11
3.2.3 *In situ* Diffuse Reflectance Infrared Fourier Transform Spectroscopy (*in situ* DRIFTS) 11

4 Results and Discussion 13
4.1 Effect of operational parameters 13
4.1.1 Temperature 13
4.1.2 Pd/Au molar ratio 14
4.2 Effect of Au core on properties of surface Pd atoms 15

4.3 Stability study over Au@Pd/Al_2O_3 with thin Pd shell thickness . . 16
4.4 *In situ* DRIFTS study over conventional supported noble metal catalysts 17

5 Conclusions and Future Work **21**

Acknowledgements **23**

References **25**

1 Introduction

Due to the increasing price of crude oil and depletion of fossil resources, as well as the environmental issues caused by combustion processes, the catalytic conversion of one-carbon compounds into high-value chemicals and clean fuels is of outmost importance [1]. This includes conversion of, *e.g.*, CO, CO_2, CH_4, CH_3OH, HCOOH and is often referred to as C1 catalysis. In the recent decades, C1 catalysis has been progressed significantly thanks to the development of new methodologies broadly, ranging from theoretical studies to industrial applications [1]. Heterogeneous catalysts play important roles in C1 catalysis, and the synthesis and development of highly efficient catalysts (high catalytic activity) with low cost has been a focus area [1]. Among the common catalysts used for C1 chemistry, noble metals supported on metal oxide carriers are known to have unique catalytic properties [2]. Such catalysts are applied to many C1 reactions, for example, CO_2 hydrogenation over Al_2O_3 supported Ir, Rh, Pt and Pd [3–7], oxidation of methane [8–22] and CO [23–30] over supported Pd and Pt catalysts.

As a member of the d-block metal groups, Pd exhibits superior performance in heterogeneous catalysis due to its $4d^{10}5s^0$ electron configuration [31]. As an example, the 2010 Nobel Prize in chemistry dealt with C-C coupling reactions facilitated by Pd catalysts in organic synthesis [32]. Further applications include CO oxidation [33, 34], catalytic methane combustion [35], petroleum cracking [36], just to name a few.

With the development of synthesis and characterization techniques, bimetallic Pd based catalysts with either alloy structure or core@shell structure have been synthesized and developed [31]. Among them, gold-palladium bimetallic nanoparticles have shown pronounced enhancement of catalytic activity compared to monometallic Au and Pd nanoparticle catalysts in many prototypical reactions, for instance, CO oxidation [33, 37], direct synthesis of hydrogen peroxide using H_2 and O_2 [38], and synthesis of vinyl acetate [39]. In recent decades, the Au and Pd bimetallic nanoparticles with core@shell structure has gained more and more interest thanks to their specific catalytic properties [31, 40–43]. The strain and ligand effects induced by adding a second metal component, which has different lattice parameters from the parent metal, trigger the complicated reaction between the two electron-rich elements, leading to the modification of surface electronic properties of the core@shell nanoparticles [44]. Hence, the catalytic activity, selectivity and stability of the nanoparticles can be enhanced [45]. Although above mentioned studies successfully demonstrated the synthesis strategy and

superior catalytic activity of Au@Pd core@shell nanoparticles, systematic insights linking the catalytic performance and the interplay of Au core and Pd shell is still lacking [46]. Especially rare are such insights in the context of thermal catalytic conversion of C1 molecules.

1.1 Objective

The present objective is to develop synthesis routes for making of Au@Pd/Al_2O_3 core@shell nanoparticles and study their catalytic performance in prototypical CO oxidation, comparing with conventional Pd and Pt based supported catalysts. In particular, batches of Au@Pd core@shell nanoparticles were synthesized by a two step seeded-growth method for which the effect of different operational parameters on the morphology of the obtained nanoparticles were investigated. Au@Pd nanoparticles with thin Pd layers (1.5 nm) were loaded onto a γ-Al_2O_3 support in order to study the nanoparticles when used for CO oxidation catalysis. Surface properties and stability of the as-prepared Au@Pd/Al_2O_3 were studied by *in situ* infrared spectroscopy. The comparison between Au@Pd/Al_2O_3 core@shell nanoparticle catalysts and conventional Pd/Al_2O_3 and Pt/Al_2O_3 monometallic catalysts are also discussed.

2 Background

2.1 Supported monometallic catalysts

Supported monometallic noble metal catalysts offer venues for various heterogeneous catalytic reactions [28]. For example, supported Pd catalysts have been widely used for total oxidation of methane [12, 17–22, 47–49] and other hydrocarbons [50, 51], supported Pt catalysts and oxide supported Au nanoparticles have been used for low temperature CO oxidation [9–11, 23–25, 27, 52, 53]. Among all kinds of supporting materials, metal oxides are the most adopted due to the possibility for tuning of the catalytic activity [54]. The properties of metal oxide supports and the metal-support interactions pose significant impacts on the catalytic performance of the catalyst. For instance, the dispersion, and consequently the catalytic behavior of the catalyst, is often influenced by the support. In general, metal oxides can be classified into two categories based on their ability to be reversible reduced: reducible metal oxides and non-reducible metal oxides. Commonly used non-reducible metal oxides supports in previous studies include La_2O_3, SiO_2, and Al_2O_3 etc. Especially, γ-Al_2O_3 have received substantial research interest due to its high specific surface area and low cost [21, 55, 56], and thus applicability. Reducible metal oxides have also been widely studied as they can participate in the catalytic reactions and induce strong metal-support interaction (MSI) that can promote catalytic conversions [52, 57, 58]. The main difference between non-reducible and reducible metal oxides is the different possibility creating oxygen vacancies, which can be useful when created close to metal particles [59].

2.1.1 Promotion by active supports

Decoding the underlying mechanisms and the promoting effects of catalyst-support interactions on a catalytic reactions is challenging but desired because it may guide how to tailor and moderate catalytic properties by the deliberate choice of included elements [52]. A general consensus is that in the metal-support system, the role of support is not simply to provide high metal dispersion but rather is a number of other effects also important [60]. The support itself may expose active sites for catalytic reactions and can provide oxygen vacancies that can promote desired reactions [61] Particularly, in some cases, the metal-support boundary seems to provide, predominantly, the active

sites [54, 62]. In addition to providing oxygen vacancies as active sites for direct participation in the reaction, there are several other possibilities that affect the catalytic activity [54], *i.e.* effect on the shape and size of the metal nanoparticles, as well as the activation procedure, by metal-support interactions (MSI) [63]; introducing strain in the metal nanoparticles [64]; or charge transfer between support and particles [65].

The promotion of catalytic activity by metal-support interaction was thought to be crucial in tuning the catalytic performance for supported metal species by affecting the size of metal species and the surface properties of some substrates [57]. The effect on metal nanoparticle sizes is the consequence of different interface energy, leading to different number of low-coordinated atoms [63]. Moreover, the lattice strain either on the support surface or at the interface between metal species and support, will influence the electronic and mechanical properties of metal species [66]. The smaller the particle size, the more significant the interatomic strain [67]. Another promotion pathway is the charge transfer between small metal clusters and the substrates, in which defect sites (vacancies, holes, etc.) are created. Those defect sites are essential to the catalytic activity and selectivity [61].

2.2 Supported bimetallic catalysts

Introduction of a second metal is also considered as an attractive way to promote catalytic activity. Compared to the corresponding monometallic catalysts, bimetallic catalysts exhibit superior performances in various applications, which can be ascribed to the modification of chemical properties induced by the addition of the second metal [68]. There are two mechanisms accounting for the chemical property changes, namely strain effects and ligand effects [44]. Strain effects are generated by lattice mismatch, which alters the adsorption energy of surface atom by changing the d-band center through the long-range effect [69]. The adsorption energy is related to binding strength. It occurs in solid solution alloy systems wherein metals with various lattice parameters are joint together, or in core@shell systems where the shell metal possesses lattice parameters different from the underlying core metal [69]. Ligand effects arise due to the change of coordination conditions of a metal atom induced by the presence of another metal, leading to the formation of hetero-nuclear metal-metal bonds, which involves charge transfer and orbital hybridization of metals [70]. However, those two effects always occur at the same time, and it is not straightforward to separate their individual effects, and experimentally observed effects are the sum of the two [71].

It is also important to understand the electronic structure of the surface atoms that interact with the adsorbates (adsorbed reactants). Generally, during the adsorption, the valence state of the adsorbate first couples with the s state of surface metal atoms, then turns to couple with metal d states, resulting in the

separation of d states into bonding and anti-bonding states [72–74]. The binding strength between an adsorbate and surface metal atom will increase with the filling of bonding d states or unfilling of anti-bonding states, and the occupancy of the anti-bonding states is only related to their location with respect to Fermi level [72, 73]. Kitchin *et al.* [71] presented a simple explanation about the electronic modification by strain and ligand effects. Basically, the d-band width, which affects the d-band energy, are found to be proportional to the interatomic bonding between the d orbitals of both surface atom and its neighboring atom. When the d-band width becomes narrower, to maintain a constant d-band filling, the average d-band energy will increase, and vice versa [71]. The combination of strain and ligand effects can be used to tune the chemical properties of the surface, potentially leading to enhancement of surface reactivity and/or catalytic activity.

2.2.1 Alloyed nanoparticles

Since the definition of various kinds of multimetallic systems is not always consistent in the literature, one should distinguish between alloyed catalysts and bimetallic catalysts. Ponec and co-authors [75] defined alloy as a metallic system, which contains two or more metal components, irrespective of their degree and mode or mixing [75]. The alloys defined in this way could form either a continuous monophasic alloys, or segregate into biphasic alloys under certain conditions (for example with temperature [75]). However, Zafeiratios *et al.* described the alloy as a chemical compound of two or more metallic parts that adopt at least partly to an ordered crystal structure differing from their corresponding constituent metals [76]. To clarify, in the present study, an alloyed system is regarded as a bimetallic system in which two different metals are joint together to form an ordered crystal structure. The enhancement of catalytic activity caused by strain and ligand effects in alloyed systems has been widely studied, especially in the treatment of vehicle emissions [33, 77–80]. In bimetallic alloy system, the strain and ligand effects are caused by size mismatch in the fcc random alloy and the redistribution of noble metal 5d states in the form of intermetallic interaction [81].

2.2.2 Core-shell nanoparticles

Another bimetallic structure is the so-called core@shell structure. The terminology ‘core-shell’ (and also denoted as ‘core@shell’) can be broadly defined as an combination of a core (inner) material and a shell (outer layer) material. Among different classes of core@shell nanoparticles, the concentric spherical core@shell nanoparticles are the most common one, in which a spherical core particle is entirely coated by a shell of another material [82]. The intrinsic aspect that distinguish core@shell from alloy system is, in the alloy system, the energy bands of the constituting metal elements are overlapped, while this is not the

case in the core@shell system [83]. In the core@shell system, when the shell metal atoms have smaller lattice parameter than the underlying core metal atoms, the surface atoms will be subjected to tensile strain. In this case, the d-band width will be broader due to the narrowing of overlapped d states between surrounding metal atoms caused by enlarged interatomic distances [69]. Moreover, as Pd has highly filled d-band ($4d^{10}5s^{0}$), the d-band center will up-shift to a higher level in order to maintain the fixed d occupancy, leading to the enhanced chemical-adsorption affinity towards some intermediates [69], especially some small adsorbates such as O, H and CO [44]. On the contrary, if the surface metal have larger lattice parameter than the underlying core metal, the surface atoms will be subjected to compressive strain, leading to increased d-orbital overlaps, which cause the broadening of d-band and lowering of average energy. Correspondingly, the affinity towards simple molecules is lower than those of the parent metal surface [44].

There are vast amount of studies on transition metal core@shell nanoparticles in the field of catalysis [84, 85]. Among these transition metal core@shell nanoparticles, well-defined Au@Pd core@shell nanoparticles have been widely studied and have been shown to exhibit excellent catalytic activity and stability. For example, Hosseini *et al.* compared the catalytic performance of total VOC oxidation over Au@Pd/TiO_2 core@shell, Pd@Au/TiO_2 core@shell and Au-Pd/TiO_2 alloy nanoparticles , and observed higher toluene and propane oxidation activity over Au@Pd/TiO_2 core@shell nanoparticles [86].

2.3 Synthesis of core@shell nanoparticles

Thanks to the development of modern techniques, tuning the core@shell nanoparticles with different chemical and physical properties could be achieved, by modifying the synthesis parameters or using various synthesis techniques. The obtained nanoparticles with, for example, different metal distribution and atomic arrangement, offers a way to tailor the catalytic activity of core@shell nanoparticles [40].

Generally, the approaches for synthesis of nanomaterials could be broadly divided into two categories, namely 'top-down' and 'bottom-up' [82]. The 'top-down' method is using external tools, such as micro-fabrication and mechanical stress, to break down the bulk materials and obtain the desired nanomaterials with different sizes and shapes [87]. However, in the 'bottom-up' method, materials are synthesized from molecular or atomic building blocks. The whole process depends on the mutual interaction and the individual chemical properties of the included elements, which determine the shape and size of the resulting material [87]. Both 'top-down' and 'bottom-up' method have their pros and cons, but the 'bottom-up' methods provide possibility producing nanoparticles with much smaller size, which has the potential to be cost-efficient considering the high control of the entire process and the minimum energy loss

[82].

In this study, the focus is on synthesizing core@shell nanoparticles using chemical methods ('bottom-up' methods). The synthesis of core@shell nanoparticles follows a two-step method: synthesis of the core, followed by synthesis of the shell [82]. Depending on the availability of the core particles, the synthesis method could be defined into two types: (i) the core nanoparticles are first prepared, washed and dried separately, then the shell material is coated onto the core particles using a proper surface modification [88–90]; (ii) the core nanoparticles are first synthesized by suitable reducing agent, then a precursor solution is added to the as-prepared core solution to form and deposit shell nanoparticles onto the core surface [91, 92]. The main difficulties during synthesis are (i) agglomeration of core particles in reaction system; (ii) preferential formation of particles of shell materials instead of coating on the core particles surfaces; (iii) control of the reaction rate [82]. Therefore, the synthesis of tailored Au@Pd is challenging.

The metallic nanoparticles are mainly obtained via reduction of the corresponding metal-salts by using external reducing agent (such as hydrogen, tannic acid, citric acid, etc.) or intrinsic redox properties of the precursor [93–95]. During the synthesis, the reaction medium, temperature, pH, and the type of reducing agents strongly affect the reaction kinetics, leading to the different sizes, shapes, chemical and physical properties. After the core nanoparticles are prepared, the precursor solution of shell materials is added into the reaction medium, followed by the addition of reducing agent, the core@shell nanoparticles are obtained.

3 Methodology

3.1 Synthesis

3.1.1 Au@Pd core@shell nanoparticles and Au@Pd/Al_2O_3 nanoparticle catalyst

The Au@Pd core@shell nanoparticles were synthesized by a two-step seeded growth method based on Pella *et al.*[96] and Hu *et al.*[97] with some modifications. First of all, the Au core nanoparticles were synthesized through reduction and nucleation. 150 mL sodium citrate was mixed with 3 mL L-ascorbic acid and 1 mL K_2CO_3 under vigorous stirring. When the temperature reached 70 °C, 1 mL 25 mM $HAuCl_4$ was injected. The color of solution changed immediately to dark red, indicating the formation of Au nanoparticles [96]. To obtain the Au@Pd core@shell nanoparticles, certain amount of H_2PdCl_4 precursor solutions were added into the as-prepared Au nanoparticles solution, the freshly prepared L-ascorbic acid was added dropwise into the solution. The color of reaction solutions changed to dark brown after the addition of L-ascorbic acid, indicating the formation of Au@Pd nanoparticles [97].

To load the Au@Pd core@shell nanoparticles onto alumina support, γ-Al_2O_3 powder was weighted and directly mixed with as-prepared Au@Pd core@shell nanoparticles solutions and stirred overnight at room temperature. The obtained slurries were centrifuged under 5000 rpm and freeze-dried. A briefly synthesis procedure is described in Figure 3.1.

Among the factors exerting effect on the characteristics of core@shell nanoparticles, reaction temperature [98] and precursor molar ratios [99] are two of the vital parameters that control the growth of core@shell nanoparticles. However, the effects of those two factors vary among different systems. Hence, to study the effect of different operational parameters during synthesis, different reaction temperatures and Au/Pd molar ratios were investigated and were listed in table 3.1. The reaction temperatures were designed to be 1, 25, and 80 °C. The molar ratio of Pd/Au were 0.31, 3.1, 31 and 310, respectively.

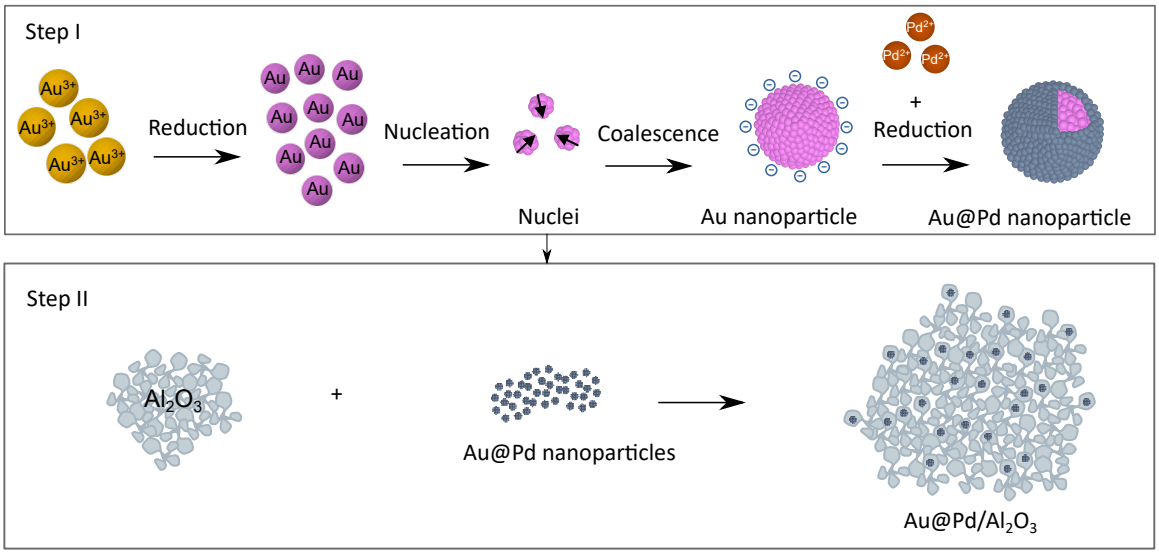

Figure 3.1: *Graphical description of synthesis of $Au@Pd/Al_2O_3$ nanoparticles.*

Sample number	Temperature (°C)	Pd/Au molar ratio
1	1	0.31
2	20	0.31
3	80	0.31
4	1	3.1
5	1	31
6	1	310

Table 3.1: *Different operational parameters.*

3.2 Characterization

3.2.1 Transmission Electron Microscopy (TEM) and High Resolution Transmission Electron Microscopy (HRTEM)

Transmission electron microscopy is a commonly used technique in the field of nanotechnology because the short wavelength of the electron with high energy could pass through the sample and achieve subnanometer resolution. During the imaging procedure, an electron beam passes through the sample, being absorbed and scattered, producing contrast and images [100]. TEM is regarded as a powerful tool to reveal the atom distribution of a nanocrystal structure even when they are passivated with polymers [79]. Nowadays, TEM is not only providing the atomic information of materials, but also chemical information about a single nanocrystal at a spatial resolution of 1 nm or even better [101].

High resolution TEM (HRTEM) is a modern TEM consisting of an illumination system, a specimen stage, an objective system, a magnification system, data

recording system, and the chemical analysis system [79]. The electron gun, which uses FEG gun as illumination source, gives high illumination current. The key to carry out the analysis of structure is the specimen stage due to its ability to perform *in situ* observation. The resolution of the image is determined by the objective lens [79].

Herein, the morphology of Au@Pd nanoparticles and Au@Pd/Al_2O_3 nanoparticle catalysts were investigated by FEI Tecnai T20 transmission electron microscopy (TEM) at 200 kV and FEI Titan 80 - 300 STEM at 300 kV. High angle annular dark field scanning transmission electron microscopy (HAADF-STEM) and energy-dispersive X-Ray spectroscopy (EDS) linescan were used for further indication of core@shell structure.

3.2.2 X-ray Diffraction (XRD)

The X-ray diffraction (X-ray diffraction (XRD) is regarded as a powerful tool that is widely used in both research and industry [102]. It is always used to quantify or qualify the crystalline phases in materials based on their diffraction patterns [102]. It is based on the constructive interference between monochromatic X-rays and a crystalline material. The source of these X-rays is a cathode ray tube. After generation, the X-rays are filtered to be monochromatic, collimated to be concentrated, and directed towards the sample. When the condition fits the Bragg's law ($2d\sin\theta = n\lambda$), the incident X-rays would interact with the sample, leading to the production of a constrictive interference as well as a diffracted ray. The Bragg's law connects the diffraction angle to the lattice spacing of crystal phase and the wavelength of electromagnetic radiation. The generated diffracted rays are detected and analyzed. By scanning the sample through a range of 2θ degrees, all the diffraction directions of the sample lattice could be obtained due to random orientation.

3.2.3 *In situ* Diffuse Reflectance Infrared Fourier Transform Spectroscopy (*in situ* DRIFTS)

Infrared spectroscopy is one of the important techniques for characterization of catalysts and catalytic reactions. It is based on measuring the absorption of infrared radiation by chemical bonds [103]. For a molecule to be capable of absorbing infrared radiation, it must have specific features, *i.e.* it must possess a change in the electric dipole moment during the vibration of the bond under consideration [104]. The vibration involves a change of either bond length (stretch) or bond angle, and the stretch mode includes symmetrical stretches and asymmetrical stretches, which depend on the feature of the molecule. [104]. For example, the CO_2 has symmetrical vibration whereas H_2O has asymmetrical vibration.

The reflection of light could mainly be divided into two cases termed specular and diffuse reflectance [105]. The specular reflection is defined as an ideal reflection, whereas diffuse reflectance refers to the reflection of light when radiation incident on the surface of the material and then is scattered in many directions rather than just one single angle as in specular reflection. The diffuse reflectance on a solid surface is not only caused by the rough surface, but also from the near surface within a layer [105]. When the light enters the material, it is absorbed, scattered and finally exited from the material. The light reflected back is recorded and the absorption can be obtained. As the light is scattered by materials multiple times, the direction at which it exit the material is random [105]. In case of diffuse reflectance infrared Fourier transform spectroscopy, the material is usually in powder, and act as its own mirror and is capable for light penetration. The advantage of this technique is easier sample preparation as compared to transmission or specular modes.

The *in situ* diffuse reflectance infrared Fourier transform spectroscopy (*in situ* DRIFTS) was used to study the interactions of gaseous species (CO and O_2) on the catalyst surface, and the effect of Au core on the electronic structure of surface Pd atoms.

4 Results and Discussion

4.1 Effect of operational parameters

4.1.1 Temperature

According to previous studies, the morphology of core@shell nanoparticles is dependent on the competition between the surface diffusion rate and the deposition rate of shell atoms, which is sensitive to the reaction temperature [91]. To investigate the effect of temperature on the morphology of Au@Pd core@shell nanoparticles, Au@Pd nanoparticles were synthesized under different temperatures, and there morphologies were characterized by transmission electron microscopy (TEM). TEM images of Au@Pd nanoparticles synthesized under 1 °C, 20 °C and 80 °C are shown in Figure 4.1. The results show that when the temperature was 1 °C, the obtained core@shell nanoparticles have an evenly distributed shell with a shell thickness ranging from 1.5 to 2 nm. However, when the temperature increased to room temperature (20 °C) or even higher (80 °C), both the thickness and the roughness of the shell increased dramatically with increasing temperature.

To understand how temperature influence the nanoparticles morphology, one should be clear about the growth mechanism of core@shell nanoparticles. As previously reported by Tan *et al.* [91], there are mainly two routes for the growth of core@shell nanoparticles: (i) nuclei coalescence, where the shell nanoparticles are formed in the solution and adsorbed onto the as-prepared core

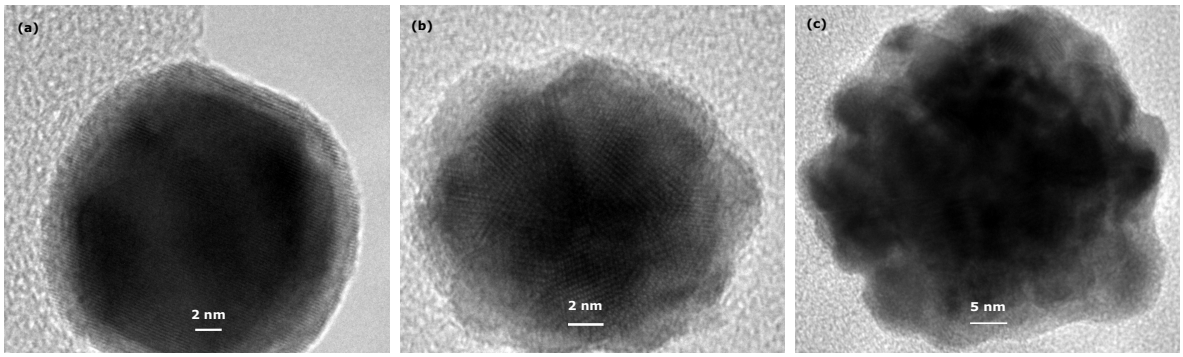

Figure 4.1: *TEM images of Au@Pd nanoparticles synthesized under different temperatures (a)* 1 ℃ *(b)* 20 ℃ *(c)* 80 ℃.

nanoparticles, and (ii) monomer attachment, where shell atoms deposit onto the core nanoparticles and then are reduced on the core surface [91] resulting in epitaxial growth. The reaction temperature plays an important role in determining the final morphology of the core@shell nanoparticles, because it controls whether the growth is under thermodynamic control or kinetic control [98]. Another study by Tan *et al.* also suggested this. By performing real-time imaging, using in situ TEM, the growth mechanism of Au@Pd core@shell nanoparticles under 25 °C and 80 °C was studied, and they figured out that under room temperature, the growth is under kinetic control, forming arrow-headed nanorods with thin Pd shell. When the temperature increased to 80 °C, the surface diffusion rate is faster, leading to a transfer of most of the Pd adatoms from tips to the side facet and the formation of a cuboical shell [92].

Guided by this information, one may propose the following mechanism for the growth of Au@Pd in the present study. In the case of using a temperature of 1 °C, the growth of Pd shell follows the monomer attachment pathway as the predominant mechanism. The $[PdCl_4]^{2-}$ anion replaces the citrate anion on the Au nanoparticle surface, and the reduction of Pd^{2+} happens on the surface. Under this circumstance, the obtained Pd shell becomes thin and evenly distributed. This hypothesis is also in line with the study from Sarkany *et al.* [106]. However, when the temperature was increased to 25 °C, the nuclei coalescence became the dominating growth pathway. Here, the Pd nanoparticles first formed in the solution, and then deposited onto the Au nanoparticle surface. The deposition rate of the formed Pd nanoparticles is faster than its surface diffusion rate, leading to rough and thick shell. Further increasing the temperature lead to even faster deposition of Pd nanoparticles. Hence, the Au@Pd core@shell nanoparticles synthesized under 80 °C possessed thicker shell than the ones synthesized under 25 °C.

4.1.2 Pd/Au molar ratio

The shell thickness, a crucial parameter affecting the electronic structure and therefore the catalytic activity of a core@shell catalyst, is also controlled by the molar ratio of Pd to Au in reaction solution [107]. Therefore, we investigated the effect of Pd/Au ratio on the morphology of the synthesized Au@Pd nanoparticles, by varying the dosage of Pd precursor during Au@Pd synthesis (the reaction solution was kept at 1 °C). Figure 4.2 shows TEM images of Au@Pd nanoparticles synthesized with different Pd/Au ratios, namely 3.12, 31.2 and 312. It is obvious that the Pd shell thickness increases with the increasing Pd/Au value. This can be attributed to the increased availability of Pd in the reaction solution for the growth of the Pd shell on the Au core at higher Pd/Au ratio. This finding is in accordance previous studies. [97]. Moreover, with high Pd/Au ratio (310), the obtained Au@Pd nanoparticles lost the smooth shell structure

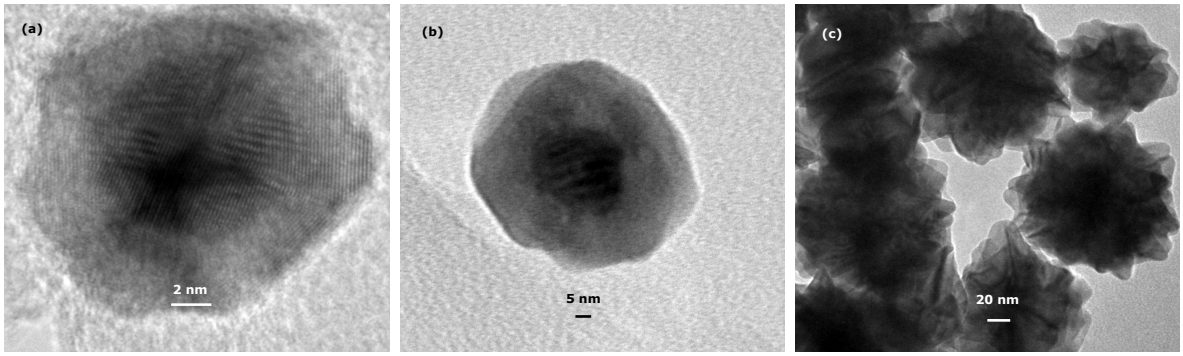

Figure 4.2: *TEM images of Au@Pd core@shell nanoparticles with different Au/Pd molar ratios (a) 0.32 (b) 0.032 and (c) 0.0032.*

and appeared a flower-like morphology. One hypothesis is that when the Pd precursor concentration was too high, the obtained Pd nanoparticles were no longer spherical, but in urchin-like shape due to the fast reaction kinetics. Hence, the urchin-like shaped Pd nanoparticles deposited onto Au surface led to flower-shaped Au@Pd nanoparticles. [108]. Another hypothesis is that the high concentration of Pd in the reaction solution disrupted the dispersion of fine Pd nanoparticles and led to agglomeration of these nanoparticles. The agglomerated Pd clusters deposited onto Au surface, resulting in flower-shaped Au@Pd nanoparticles [109].

4.2 Effect of Au core on properties of surface Pd atoms

In order to study how the Au core would affect the electronic structure of shell Pd atoms, the Au@Pd/Al_2O_3 nanoparticles with 1.5 nm Pd thickness (around 5 atomic layers) were used as the model catalysts, because thicker shell would cover the interactions of both Au and Pd. [110, 111]. The catalytic activities of the model bimetallic Au@Pd catalyst and the Pd catalyst were studied by *in situ* DRIFTS using CO as probing molecule. CO adsorption experiments under descending temperature ranging from 198 °C to 33 °C were performed, and the DRIFTS spectra are shown in Figure 4.3. The peaks located at 2082 cm^{-1} in both Figure 4.3(a) and (b) are assigned to linearly bonded CO species on Pd atoms, while the peaks located at 1997 cm^{-1} in Figure 4.3(a) and 1985 cm^{-1} in Figure 4.3(b) are referred to bridge-bonded CO species on Pd atoms [112]. For Au@Pd/Al_2O_3 nanoparticles, the bridge bonded CO peaks started to show up from 176 °C in a broad shape, whose peak intensity increased with the descending temperature. Comparing the spectra under 33 °C of Au@Pd/Al_2O_3 to Pd/Al_2O_3, no notable change of linear bounded peaks was observed, while the bridge-bonded CO species had a blue-shift of 12 cm^{-1}. One explanation is

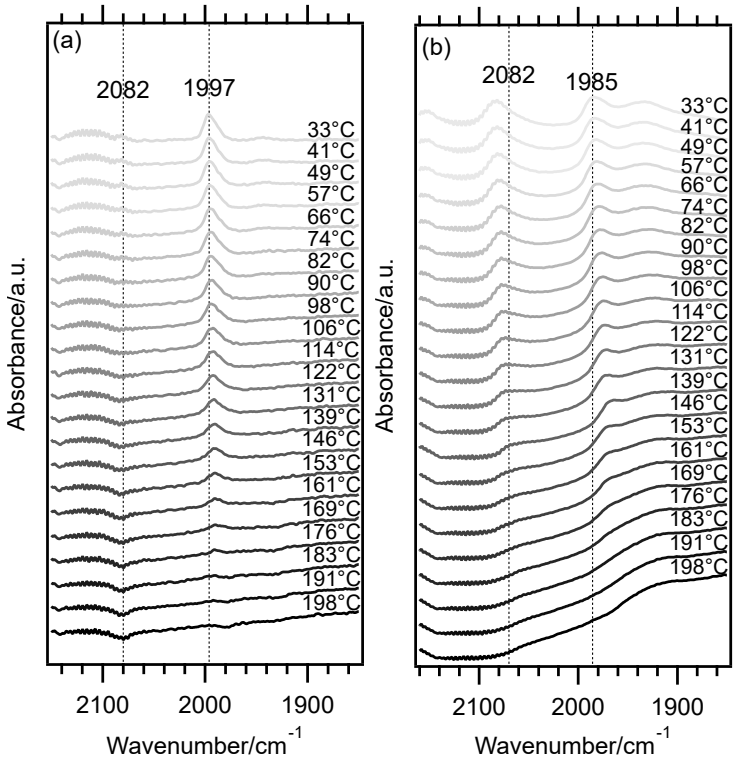

Figure 4.3: *DRIFTS spectra of CO adsorption experiment over (a) Au@Pd/Al_2O_3 nanoparticle catalyst. (b) Pd/Al_2O_3 nanoparticle catalyst.*

the electrons transferred from Pd to Au core, leading to the weakening of back donation from Pd to CO. However, as the abundance of linearly bonded CO species was low, the change of linear peak was negligible.

4.3 Stability study over Au@Pd/Al_2O_3 with thin Pd shell thickness

The physical and chemical properties of nanoparticles and therefore their catalytic activities are strongly dependent on their compositions and configurations, which influence the defects density at the nanoparticle surfaces [113]. Hence, it is very important to investigate the structure stability of the Au@Pd/Al_2O_3 during the CO oxidation experiment. Figure 4.4 shows TEM images, HAADF-STEM images, and EDS linescan profiles across the surface (orange line) of as-prepared Au@Pd/Al_2O_3 nanoparticle catalyst and the catalyst collected after CO ignition and extinction experiments. The TEM images suggest no notable agglomeration of Au@Pd nanoparticles on Al_2O_3 surface. Moreover, the HAADF-STEM images as well as EDS linescan profile suggest that the core@shell structure was remained upon exposed to CO oxidation condition, which indicate good structural stability of Au@Pd/Al_2O_3 core@shell nanoparticle catalyst.

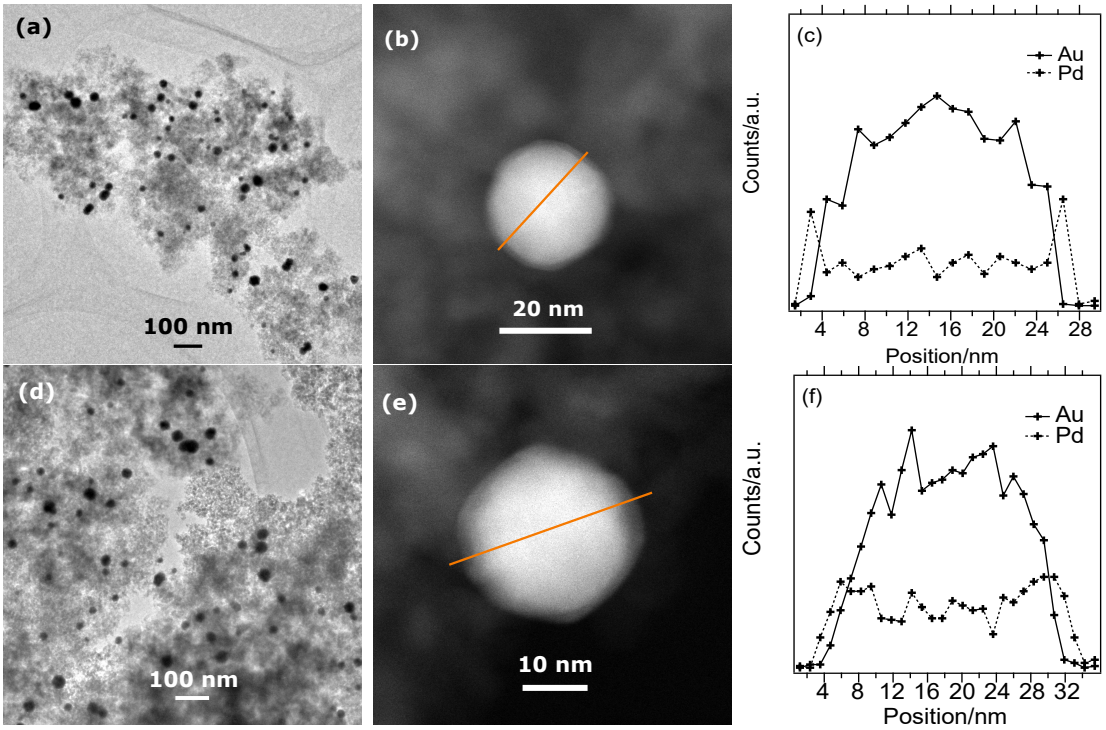

Figure 4.4: *(a) TEM image of as-prepared Au@Pd/Al_2O_3 nanoparticles. (b) HAADF-STEM image of as-prepared Au@Pd/Al_2O_3 nanoparticles. (c) Linescan profile of Au@Pd/Al_2O_3 nanoparticles collected after DRIFTS experiment. (d) TEM image of Au@Pd/Al_2O_3 nanoparticles collected after DRIFTS experiment. (e) HAADF-STEM image of as-prepared Au@Pd/Al_2O_3 nanoparticles. (f) Linescan profile of Au@Pd/Al_2O_3 nanoparticles collected after DRIFTS.*

4.4 *In situ* DRIFTS study over conventional supported noble metal catalysts

When exploring the advantages of bimetallic core@shell system, it is also important to have knowledge about the catalytic performance of traditional noble metal catalysts for exhausted gases treatment (CO oxidation), and to compare the catalytic behavior of core@shell system to them. Among all traditional noble metal based catalysts, the Pd and Pt based catalyst are the most common ones that has been widely used for CO purification from vehicle emission [114]. CO is excessively adsorbed on both Pd and Pt surface, which causes the self-poisoning and the O_2 is unable to be dissociated and activated on the catalyst surface, improving the temperature could assist the CO oxidation reaction to happen [115]. In spite of this, the interaction between CO species and the metal surface during CO oxidation is still different between Pd and Pt based catalyst. Hence, a comparison of Au@Pd/Al_2O_3, Pd/Al_2O_3 and Pt/Al_2O_3 was carried out in our study.

CO oxidation (extinction) experiment over Pd/Al_2O_3 and Pt/Al_2O_3 were

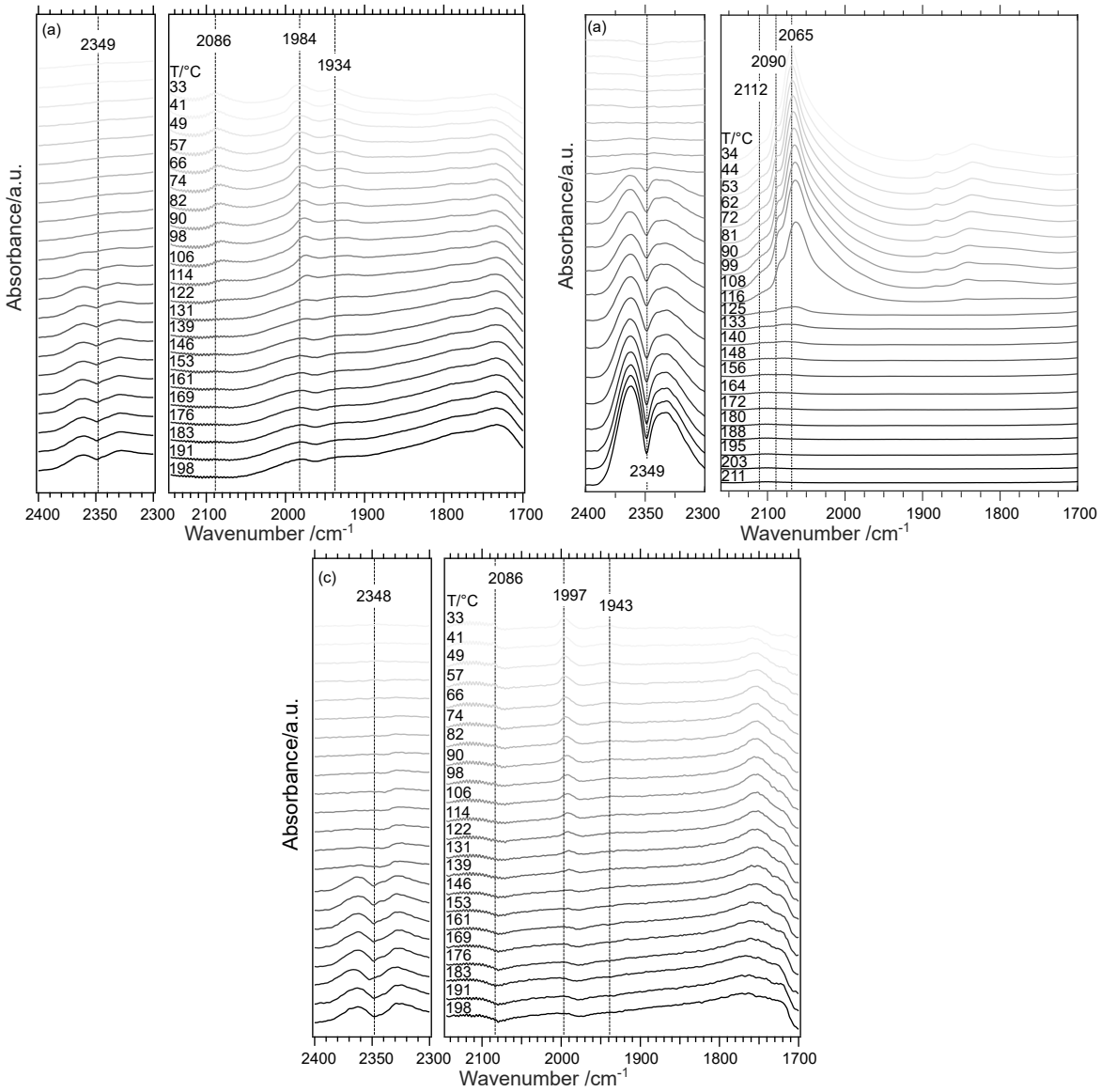

Figure 4.5: *DRIFTS spectra of CO oxidation (extinction) over (a)Pd/Al_2O_3 from* 198 ℃ *to* 33 ℃*; (b)Pt/Al_2O_3 from* 211 ℃ *to* 34 ℃*; (c) $Au@Pd/Al_2O_3$.*

performed under descending temperature using *in situ* DRIFTS. Figure 4.5 (a) shows the DRIFTS spectra of CO oxidation (extinction) experiment over Pd/Al_2O_3 catalyst from 198 °C to 33 °C. The peak located at 2349 cm^{-1} is assigned to CO_2 in gas phase, and starts to show up from 198 °C and vanish at 122 °C, where the linearly and bridge-bonded CO species started to be observed. The intensity for both the linear and bridge bonded CO peaks increased with the decreasing temperature, indicating higher CO coverage. Figure 4.5 (b) shows the CO oxidation (extinction) spectra of Pt/Al_2O_3 catalyst (from manuscript II). The result shows similar increasing trend for the intensity of linearly bonded CO peak when decreasing the temperature. However, an abrupt increase of linearly-bonded

CO species at 116 °C, and the production of CO_2 was also encountered with an sudden diminution, which was caused by the sudden build-up of adsorbed CO species on Pt surface.

As for DRIFTS spectra of CO extinction experiment over Au@Pd/Al_2O_3 in Figure 4.5(c), no drastic increasing of linear bonded CO species were observed when decreasing the temperature, and they are constant throughout the whole experiment procedure.

5 Conclusions and Future Work

Au@Pd core@shell nanoparticles with different shell/core ratio were synthesized by a two-step seeded-growth method, and were loaded onto γ-Al_2O_3 support. Among all the operational parameters that affect the morphology of Au@Pd nanoparticles, reaction temperature and Pd/Au molar ratio were investigated. Results suggest that at 1 °C, very thin and evenly distributed Pd shell could be obtained, while when increasing the temperature to 25 °C and 80 °C, the Pd shell became thicker and possessed rougher surface. The reasons lie in the competition between the deposition rate of pd nanoparticles onto the surface and their surface diffusion rate on Au core surface. Moreover, the Pd shell thickness and roughness also increased with the increasing Pd/Au molar ratio. When the value reached 310, the obtained Au@Pd nanoparticles were in flower shape, which was attributed to the larger amount of Pd nanoparticles and the lack of stabilizer.

To study the electronic structure of Pd shell under the effect of Au core, the Au@Pd/Al_2O_3 with thin shell thickness (around 1.5 nm) was chosen as the model catalyst. The alteration of electron arrangement in Pd d state was probed by CO adsorption experiment using *in situ* DRIFTS under descending temperature from 198 °C to 33 °C. The obtained spectra were compared to the DRIFTS spectra of CO adsorption over Pd/Al_2O_3. A blue-shift of bridge-bonded CO on Pd peak was observed. The reasons could be the net charge flew from Pd to Au, leading to the weakening of back-donation from Pd to CO. However, the change of linearly bonded CO peak was negligible. That is due to little abundant of linearly adsorbed CO on Pd surface.

In addition, the structural stability of Au@Pd/Al_2O_3 nanoparticles during CO oxidation process was investigated by TEM, HAADF-STEM, and EDS linescan. No significant agglomeration was observed upon the CO oxidation process, and the core@shell structure remained by the indication of EDS linescan profile of the sample collected after DRIFTS experiment.

The comparison of CO oxidation (extinction) behaviors over traditional Pd/Al_2O_3 and Pt/Al_2O_3 nanoparticle catalysts was also performed. The obtained CO adsorption behaviors were different. The intensity of linear CO adsorption peaks on Pd/Al_2O_3 catalyst increased gradually with the decreasing temperature, while the peaks on Pt/Al_2O_3 had a drastic change that was caused by sudden build-up of surface CO species.

The upcoming research will focus mainly on Au@Pd core@shell nanoparticles and traditional Pd based catalyst. The core@shell architecture by controlling

strain effect is regarded as an effective way to tune the electronic structure of shell atoms for enhanced catalytic activity [107]. There are several ways to control the strain effect, among them, varying the core/shell ratio is of great interest. It is known that the smaller the particle size, the more significant the interatomic strain [67]. However, to the best of our knowledge, studies are mainly focusing on the effect of diverse shell thickness on the catalytic performance, little studies about the effect of core size have been performed, especially the one relating the strain effect to the core size under thermal induced catalytic conditions [116]. With this purpose, we plan to synthesize Au@Pd core@shell nanoparticles with fixed Pd shell thickness (around 1.5 nm) while varying the size of Au core. The as-prepared Au@Pd will be loaded onto γ-alumina support, and be investigated by in-DRIFTS.

In parallel to this, to better understand the difference of CO oxidation procedure between traditional Pd based catalysts and Pt based catalysts, as well as the promotion effect induced by different support, a comparison study on Pd/CeO_2 and Pt/CeO_2 will be performed.

Acknowledgments

The project is financially supported by the Swedish Research Council. The study was mainly performed at applied chemistry, and partly at Chalmers Materials Analysis Laboratory (CMAL).

I would like to thank my main supervisor Per-Anders Carlsson, co-supervisor Hanna Härelind and my examiner Martin Andersson. Thank you for helping me throughout three years. Thank you that you always appreciated my work, gave me feedbacks and guidance, and lots of confidence on my research.

My colleague Andreas Schaefer, thank you for always giving me help on the equipment and the data analysis. Jojo, thank you sincerely. Your accompany and support mean a lot to me. Ghodsieh, thank you for always trying to bring me together to the gym, I will join you for sure during the rest of my PhD life. My office mate Maja, thank you for the daily talk, I enjoy the time we spend together. Felix, Alex, Chris, Guido, I am really glad to be groupmates with you, and I really enjoy the discussions with you.

I would also like to thank to Stefan and Ludvig from CMAL. Thank you for always assisting me on the transmission electron microscopy with a lot patience.

Many thanks to all my friend and colleagues in the department. I do appreciated all the nice moments we have. Thank you Yin, Cansu, Qingdian, Mariana, Shensheng, Ruowei, Jin, Yifei, Zhihang, Xueting, Ying, Chenyu, Peter, Carl-Robert, Johanna.

Last but not the least, I would like to express many thanks and love to my dear parents and all my family. Thank you for supporting me over the last 28 years. You always respect my choices and give me so much love and supports that light up my life.

References

[1] Bao, J.; Yang, G.; Yoneyama, Y.; Tsubaki, N. Significant advances in C1 catalysis: highly efficient catalysts and catalytic reactions. *ACS Catalysis* **2019**, *9*, 3026–3053.

[2] De Souza, P. M.; Rabelo-Neto, R. C.; Borges, L. E.; Jacobs, G.; Davis, B. H.; Resasco, D. E.; Noronha, F. B. Hydrodeoxygenation of phenol over Pd catalysts. Effect of support on reaction mechanism and catalyst deactivation. *ACS Catalysis* **2017**, *7*, 2058–2073.

[3] Solymosi, F.; Erdőhelyi, A. Hydrogenation of CO_2 to CH_4 over alumina-supported noble metals. *Journal of Molecular Catalysis* **1980**, *8*, 471–474.

[4] Martin, N. M.; Velin, P.; Skoglundh, M.; Bauer, M.; Carlsson, P.-A. Catalytic hydrogenation of CO_2 to methane over supported Pd, Rh and Ni catalysts. *Catalysis Science & Technology* **2017**, *7*, 1086–1094.

[5] Martin, N. M.; Hemmingsson, F.; Wang, X.; Merte, L. R.; Hejral, U.; Gustafson, J.; Skoglundh, M.; Meira, D. M.; Dippel, A.-C.; Gutowski, O., et al. Structure–function relationship during CO_2 methanation over Rh/Al_2O_3 and Rh/SiO_2 catalysts under atmospheric pressure conditions. *Catalysis Science & Technology* **2018**, *8*, 2686–2696.

[6] Martin, N. M.; Hemmingsson, F.; Schaefer, A.; Ek, M.; Merte, L. R.; Hejral, U.; Gustafson, J.; Skoglundh, M.; Dippel, A.-C.; Gutowski, O., et al. Structure–function relationship for CO_2 methanation over ceria supported Rh and Ni catalysts under atmospheric pressure conditions. *Catalysis Science & Technology* **2019**, *9*, 1644–1653.

[7] Hemmingsson, F.; Schaefer, A.; Skoglundh, M.; Carlsson, P.-A. CO_2 methanation over Rh/CeO_2 studied with infrared modulation excitation spectroscopy and phase sensitive detection. *Catalysts* **2020**, *10*, 601.

[8] Cullis, C.; Willatt, B. Oxidation of methane over supported precious metal catalysts. *Journal of Catalysis* **1983**, *83*, 267–285.

[9] Becker, E.; Carlsson, P.-A.; Grönbeck, H.; Skoglundh, M. Methane oxidation over alumina supported platinum investigated by time-resolved in situ XANES spectroscopy. *Journal of Catalysis* **2007**, *252*, 11–17.

[10] Becker, E.; Carlsson, P.-A.; Skoglundh, M. Methane oxidation over alumina and ceria supported platinum. *Topics in Catalysis* **2009**, *52*, 1957–1961.

[11] Becker, E.; Carlsson, P.-A.; Kylhammar, L.; Newton, M. A.; Skoglundh, M. In situ spectroscopic investigation of low-temperature oxidation of methane over alumina-supported platinum during periodic operation. *The Journal of Physical Chemistry C* **2011**, *115*, 944–951.

[12] Carlsson, P.-A.; Fridell, E.; Skoglundh, M. Methane oxidation over Pt/Al_2O_3 and Pd/Al_2O_3 catalysts under transient conditions. *Catalysis Letters* **2007**, *115*, 1–7.

[13] Carlsson, P.-A.; Skoglundh, M. Low-temperature oxidation of carbon monoxide and methane over alumina and ceria supported platinum catalysts. *Applied Catalysis B: Environmental* **2011**, *101*, 669–675.

[14] Fouladvand, S.; Schernich, S.; Libuda, J.; Grönbeck, H.; Pingel, T.; Olsson, E.; Skoglundh, M.; Carlsson, P.-A. Methane oxidation over Pd supported on ceria–alumina under rich/lean cycling conditions. *Topics in Catalysis* **2013**, *56*, 410–415.

[15] Fouladvand, S.; Skoglundh, M.; Carlsson, P.-A. A transient in situ infrared spectroscopy study on methane oxidation over supported Pt catalysts. *Catalysis Science & Technology* **2014**, *4*, 3463–3473.

[16] Fouladvand, S.; Skoglundh, M.; Carlsson, P.-A. Unsteady-state operation of supported platinum catalysts for high conversion of methane. *Chemical Engineering Journal* **2016**, *292*, 321–325.

[17] Nilsson, J.; Carlsson, P.-A.; Fouladvand, S.; Martin, N. M.; Gustafson, J.; Newton, M. A.; Lundgren, E.; Gronbeck, H.; Skoglundh, M. Chemistry of supported palladium nanoparticles during methane oxidation. *ACS Catalysis* **2015**, *5*, 2481–2489.

[18] Nilsson, J.; Carlsson, P.-A.; Martin, N. M.; Adams, E. C.; Agostini, G.; Grönbeck, H.; Skoglundh, M. Methane oxidation over Pd/Al_2O_3 under rich/lean cycling followed by operando XAFS and modulation excitation spectroscopy. *Journal of Catalysis* **2017**, *356*, 237–245.

[19] Nilsson, J.; Carlsson, P.-A.; Martin, N. M.; Velin, P.; Meira, D. M.; Grönbeck, H.; Skoglundh, M. Oxygen step-response experiments for methane oxidation over Pd/Al_2O_3: An in situ XAFS study. *Catalysis Communications* **2018**, *109*, 24–27.

[20] Velin, P.; Ek, M.; Skoglundh, M.; Schaefer, A.; Raj, A.; Thompsett, D.; Smedler, G.; Carlsson, P.-A. Water inhibition in methane oxidation over alumina supported palladium catalysts. *The Journal of Physical Chemistry C* **2019**, *123*, 25724–25737.

[21] Velin, P.; Florén, C.-R.; Skoglundh, M.; Raj, A.; Thompsett, D.; Smedler, G.; Carlsson, P.-A. Palladium dispersion effects on wet methane oxidation kinetics. *Catalysis Science & Technology* **2020**, *10*, 5460–5469.

[22] Velin, P.; Hemmingsson, F.; Schaefer, A.; Skoglundh, M.; Lomachenko, K. A.; Raj, A.; Thompsett, D.; Smedler, G.; Carlsson, P.-A. Hampered PdO Redox Dynamics by Water Suppresses Lean Methane Oxidation over Realistic Palladium Catalysts. *ChemCatChem* **2021**, *13*, 3765–3771.

[23] Carlsson, P.-A.; Thormählen, P.; Skoglundh, M.; Persson, H.; Fridell, E.; Jobson, E.; Andersson, B. Periodic control for improved low-temperature catalytic activity. *Topics in Catalysis* **2001**, *16*, 343–347.

[24] Carlsson, P.-A.; Skoglundh, M.; Fridell, E.; Jobson, E.; Andersson, B. Induced low temperature catalytic ignition by transient changes in the gas composition. *Catalysis Today* **2002**, *73*, 307–313.

[25] Carlsson, P.-A.; Skoglundh, M.; Thormählen, P.; Andersson, B. Low-temperature CO oxidation over a Pt/Al_2O_3 monolith catalyst investigated by step-response experiments and simulations. *Topics in Catalysis* **2004**, *30*, 375–381.

[26] Carlsson, P.-A.; Österlund, L.; Thormählen, P.; Palmqvist, A.; Fridell, E.; Jansson, J.; Skoglundh, M. A transient in situ FTIR and XANES study of CO oxidation over Pt/Al_2O_3 catalysts. *Journal of Catalysis* **2004**, *226*, 422–434.

[27] Carlsson, P.-A.; Zhdanov, V. P.; Skoglundh, M. Self-sustained kinetic oscillations in CO oxidation over silica-supported Pt. *Physical Chemistry Chemical Physics* **2006**, *8*, 2703–2706.

[28] Satsuma, A.; Osaki, K.; Yanagihara, M.; Ohyama, J.; Shimizu, K. Activity controlling factors for low-temperature oxidation of CO over supported Pd catalysts. *Applied Catalysis B: Environmental* **2013**, *132*, 511–518.

[29] Martin, N. M.; Skoglundh, M.; Smedler, G.; Raj, A.; Thompsett, D.; Velin, P.; Martinez-Casado, F. J.; Matej, Z.; Balmes, O.; Carlsson, P.-A. CO Oxidation and Site Speciation for Alloyed Palladium–Platinum Model Catalysts Studied by in Situ FTIR Spectroscopy. *The Journal of Physical Chemistry C* **2017**, *121*, 26321–26329.

[30] Wang, A.; Lindgren, K.; Di, M.; Bernin, D.; Carlsson, P.-A.; Thuvander, M.; Olsson, L. Insight into hydrothermal aging effect on Pd sites over Pd/LTA and Pd/SSZ-13 as PNA and CO oxidation monolith catalysts. *Applied Catalysis B: Environmental* **2020**, *278*, 119315.

[31] Fan, J.; Du, H.; Zhao, Y.; Wang, Q.; Liu, Y.; Li, D.; Feng, J. Recent progress on rational design of bimetallic Pd based catalysts and their advanced catalysis. *ACS Catalysis* **2020**, *10*, 13560–13583.

[32] Miyaura, N.; Suzuki, A. Palladium-catalyzed cross-coupling reactions of organoboron compounds. *Chemical Reviews* **1995**, *95*, 2457–2483.

[33] Xu, J.; White, T.; Li, P.; He, C.; Yu, J.; Yuan, W.; Han, Y.-F. Biphasic Pd- Au alloy catalyst for low-temperature CO oxidation. *Journal of the American Chemical Society* **2010**, *132*, 10398–10406.

[34] Suo, Z.; Ma, C.; Jin, M.; He, T.; An, L. The active phase of Au–Pd/Al_2O_3 for CO oxidation. *Catalysis Communications* **2008**, *9*, 2187–2190.

[35] Bunting, R. J.; Cheng, X.; Thompson, J.; Hu, P Amorphous surface PdO X and its activity toward methane combustion. *ACS Catalysis* **2019**, *9*, 10317–10323.

[36] Wildschut, J.; Mahfud, F. H.; Venderbosch, R. H.; Heeres, H. J. Hydrotreatment of fast pyrolysis oil using heterogeneous noble-metal catalysts. *Industrial & Engineering Chemistry Research* **2009**, *48*, 10324–10334.

[37] Maroun, F; Ozanam, F; Magnussen, O.; Behm, R. The role of atomic ensembles in the reactivity of bimetallic electrocatalysts. *Science* **2001**, *293*, 1811–1814.

[38] Landon, P.; Collier, P. J.; Papworth, A. J.; Kiely, C. J.; Hutchings, G. J. Direct formation of hydrogen peroxide from H_2/O_2 using a gold catalyst. *Chemical Communications* **2002**, 2058–2059.

[39] Chen, M.; Kumar, D.; Yi, C.-W.; Goodman, D. W. The promotional effect of gold in catalysis by palladium-gold. *Science* **2005**, *310*, 291–293.

[40] Van der Hoeven, J. E.; Jelic, J.; Olthof, L. A.; Totarella, G.; van Dijk-Moes, R. J.; Krafft, J.-M.; Louis, C.; Studt, F.; van Blaaderen, A.; de Jongh, P. E. Unlocking synergy in bimetallic catalysts by core–shell design. *Nature Materials* **2021**, 1–5.

[41] Chen, D.; Li, C.; Liu, H.; Ye, F.; Yang, J. Core-shell Au@ Pd nanoparticles with enhanced catalytic activity for oxygen reduction reaction via core-shell Au@ Ag/Pd constructions. *Scientific Reports* **2015**, *5*, 1–9.

[42] Hsu, C.; Huang, C.; Hao, Y.; Liu, F. Au/Pd core-shell nanoparticles with varied hollow Au cores for enhanced formic acid oxidation. *Nanoscale Research Letters* **2013**, *8*, 1–7.

[43] Kuo, C.-H.; Lamontagne, L. K.; Brodsky, C. N.; Chou, L.-Y.; Zhuang, J.; Sneed, B. T.; Sheehan, M. K.; Tsung, C.-K. The effect of lattice strain on the catalytic properties of Pd nanocrystals. *ChemSusChem* **2013**, *6*, 1993–2000.

[44] Kitchin, J.; Nørskov, J. K.; Barteau, M.; Chen, J. Modification of the surface electronic and chemical properties of Pt (111) by subsurface 3d transition metals. *The Journal of Chemical Physics* **2004**, *120*, 10240–10246.

[45] Tedsree, K.; Li, T.; Jones, S.; Chan, C. W. A.; Yu, K. M. K.; Bagot, P. A.; Marquis, E. A.; Smith, G. D.; Tsang, S. C. E. Hydrogen production from formic acid decomposition at room temperature using a Ag–Pd core–shell nanocatalyst. *Nature Nanotechnology* **2011**, *6*, 302–307.

[46] Celorrio, V.; Quaino, P. M.; Santos, E.; Flórez-Montaño, J.; Humphrey, J. J. L.; Guillén-Villafuerte, O.; Plana, D.; Lázaro, M. J.; Pastor, E.; Fermín, D. J. Strain Effects on the Oxidation of CO and HCOOH on Au–Pd Core–Shell Nanoparticles. *ACS Catalysis* **2017**, *7*, 1673–1680.

[47] Maeda, H; Kinoshita, Y; Reddy, K.; Muto, K; Komai, S; Katada, N; Niwa, M Activity of palladium loaded on zeolites in the combustion of methane. *Applied Catalysis A: General* **1997**, *163*, 59–69.

[48] Ciuparu, D.; Pfefferle, L. Support and water effects on palladium based methane combustion catalysts. *Applied Catalysis A: General* **2001**, *209*, 415–428.

[49] Mayernick, A. D.; Janik, M. J. Methane oxidation on Pd–Ceria: A DFT study of the mechanism over $\mathrm{PdxCe_1} - x\mathrm{O_2}$, Pd, and PdO. *Journal of Catalysis* **2011**, *278*, 16–25.

[50] Burch, R; Loader, P.; Urbano, F. Some aspects of hydrocarbon activation on platinum group metal combustion catalysts. *Catalysis Today* **1996**, *27*, 243–248.

[51] Kim, K. B.; Kim, M. K.; Kim, Y. H.; Song, K. S.; Park, E. D. Propane combustion over supported Pd catalysts. *Research on Chemical Intermediates* **2010**, *36*, 603–611.

[52] Visser, T.; Nijhuis, T. A.; Van Der Eerden, A. M.; Jenken, K.; Ji, Y.; Bras, W.; Nikitenko, S.; Ikeda, Y.; Lepage, M.; Weckhuysen, B. M. Promotion effects in the oxidation of CO over zeolite-supported Pt nanoparticles. *The Journal of Physical Chemistry B* **2005**, *109*, 3822–3831.

[53] Bond, G. C.; Louis, C.; Thompson, D., *Catalysis by gold*; World Scientific: 2006; Vol. 6.

[54] Widmann, D.; Liu, Y.; Schüth, F.; Behm, R. J. Support effects in the Au-catalyzed CO oxidation–Correlation between activity, oxygen storage capacity, and support reducibility. *Journal of Catalysis* **2010**, *276*, 292–305.

[55] Eguchi, K.; Arai, H. Low temperature oxidation of methane over Pd-based catalysts—effect of support oxide on the combustion activity. *Applied Catalysis A: General* **2001**, *222*, 359–367.

[56] Kim, D. H.; Lim, M. S. Kinetics of selective CO oxidation in hydrogen-rich mixtures on Pt/alumina catalysts. *Applied Catalysis A: General* **2002**, *224*, 27–38.

[57] Lou, Y.; Xu, J.; Zhang, Y.; Pan, C.; Dong, Y.; Zhu, Y. Metal-support interaction for heterogeneous catalysis: from nanoparticles to single atoms. *Materials Today Nano* **2020**, 100093.

[58] Duan, S.; Senkan, S. Catalytic conversion of ethanol to hydrogen using combinatorial methods. *Industrial & Engineering Chemistry Research* **2005**, *44*, 6381–6386.

[59] Fierro-Gonzalez, J. C.; Gates, B. C. Mononuclear AuIII and AuI complexes bonded to zeolite NaY: catalysts for CO oxidation at 298 K. *The Journal of Physical Chemistry B* **2004**, *108*, 16999–17002.

[60] Tauster, S.; Fung, S.; Garten, R. L. Strong metal-support interactions. Group 8 noble metals supported on titanium dioxide. *Journal of the American Chemical Society* **1978**, *100*, 170–175.

[61] He, Z.; Yang, M.; Wang, X.; Zhao, Z.; Duan, A. Effect of the transition metal oxide supports on hydrogen production from bio-ethanol reforming. *Catalysis Today* **2012**, *194*, 2–8.

[62] Hayek, K; Kramer, R; Paál, Z Metal-support boundary sites in catalysis. *Applied Catalysis A: General* **1997**, *162*, 1–15.

[63] Janssens, T. V.; Carlsson, A.; Puig-Molina, A.; Clausen, B. S. Relation between nanoscale Au particle structure and activity for CO oxidation on supported gold catalysts. *Journal of Catalysis* **2006**, *240*, 108–113.

[64] Mavrikakis, M.; Stoltze, P.; Nørskov, J. K. Making gold less noble. *Catalysis Letters* **2000**, *64*, 101–106.

[65] Sanchez, A; Abbet, S; Heiz, U; Schneider, W.-D.; Häkkinen, H; Barnett, R.; Landman, U. When gold is not noble: nanoscale gold catalysts. *The Journal of Physical Chemistry A* **1999**, *103*, 9573–9578.

[66] Smith, A. M.; Mohs, A. M.; Nie, S. Tuning the optical and electronic properties of colloidal nanocrystals by lattice strain. *Nature Nanotechnology* **2009**, *4*, 56–63.

[67] Wang, S.; Omidvar, N.; Marx, E.; Xin, H. Coordination numbers for unraveling intrinsic size effects in gold-catalyzed CO oxidation. *Physical Chemistry Chemical Physics* **2018**, *20*, 6055–6059.

[68] Sinfelt, J. H.; Meitzner, G. D. X-ray absorption edge studies of the electronic structure of metal catalysts. *Accounts of Chemical Research* **1993**, *26*, 1–6.

[69] Xia, Z.; Guo, S. Strain engineering of metal-based nanomaterials for energy electrocatalysis. *Chemical Society Reviews* **2019**, *48*, 3265–3278.

[70] Yi, C.-W.; Luo, K; Wei, T; Goodman, D. The composition and structure of Pd- Au surfaces. *The Journal of Physical Chemistry B* **2005**, *109*, 18535–18540.

[71] Kitchin, J. R.; Nørskov, J. K.; Barteau, M. A.; Chen, J. Role of strain and ligand effects in the modification of the electronic and chemical properties of bimetallic surfaces. *Physical Review Letters* **2004**, *93*, 156801.

[72] Strasser, P.; Koh, S.; Anniyev, T.; Greeley, J.; More, K.; Yu, C.; Liu, Z.; Kaya, S.; Nordlund, D.; Ogasawara, H., et al. Lattice-strain control of the activity in dealloyed core–shell fuel cell catalysts. *Nature Chemistry* **2010**, *2*, 454–460.

[73] Nilsson, A; Pettersson, L.; Hammer, B; Bligaard, T; Christensen, C.; Nørskov, J. The electronic structure effect in heterogeneous catalysis. *Catalysis Letters* **2005**, *100*, 111–114.

[74] Hammer, B.; Nørskov, J. K. Theoretical surface science and catalysis—calculations and concepts. *Advances in Catalysis* **2000**, *45*, 71–129.

[75] Ponec, V.; Bond, G. C., *Catalysis by metals and alloys*; Elsevier: 1995; Vol. 95.

[76] Zafeiratos, S.; Piccinin, S.; Teschner, D. Alloys in catalysis: phase separation and surface segregation phenomena in response to the reactive environment. *Catalysis Science & Technology* **2012**, *2*, 1787–1801.

[77] Hu, W.; Wu, Y.; Chen, J.; Qu, P.; Zhong, L.; Chen, Y. Methane Combustion with a Pd–Pt Catalyst Stabilized by Magnesia–Alumina Spinel in a High-Humidity Feed. *Industrial & Engineering Chemistry Research* **2020**, *59*, 11170–11176.

[78] Liu, G.; Walsh, A. G.; Zhang, P. Synergism of iron and platinum species for low-temperature CO oxidation: from two-dimensional surface to nanoparticle and single-atom catalysts. *The Journal of Physical Chemistry Letters* **2020**, *11*, 2219–2229.

[79] Wang, Z. Transmission electron microscopy of shape-controlled nanocrystals and their assemblies. *The Journal of Physical Chemistry B* **2000**, *104*, 1153–1175.

[80] Chan, Y. T.; Siddharth, K.; Shao, M. Investigation of cubic Pt alloys for ammonia oxidation reaction. *Nano Research* **2020**, *13*, 1920–1927.

[81] Chen, J.; Finfrock, Y. Z.; Wang, Z.; Sham, T.-K. Strain and ligand effects in Pt-Ni alloys studied by valence-to-core X-ray emission spectroscopy. *Scientific Reports* **2021**, *11*, 1–8.

[82] Ghosh Chaudhuri, R.; Paria, S. Core/shell nanoparticles: classes, properties, synthesis mechanisms, characterization, and applications. *Chemical Reviews* **2012**, *112*, 2373–2433.

[83] Borah, R.; Verbruggen, S. W. Silver–gold bimetallic alloy versus core–shell nanoparticles: Implications for plasmonic enhancement and photothermal applications. *The Journal of Physical Chemistry C* **2020**, *124*, 12081–12094.

[84] Zeng, J.; Yang, J.; Lee, J. Y.; Zhou, W. Preparation of carbon-supported core- shell Au- Pt nanoparticles for methanol oxidation reaction: The promotional effect of the Au Core. *The Journal of Physical Chemistry B* **2006**, *110*, 24606–24611.

[85] Yin, H.; Ma, Z.; Chi, M.; Dai, S. Heterostructured catalysts prepared by dispersing Au@ Fe2O3 core–shell structures on supports and their performance in CO oxidation. *Catalysis Today* **2011**, *160*, 87–95.

[86] Hosseini, M; Barakat, T; Cousin, R; Aboukaïs, A; Su, B.-L.; De Weireld, G; Siffert, S Catalytic performance of core–shell and alloy Pd–Au nanoparticles for total oxidation of VOC: The effect of metal deposition. *Applied Catalysis B: Environmental* **2012**, *111*, 218–224.

[87] Gawande, M. B.; Goswami, A.; Asefa, T.; Guo, H.; Biradar, A. V.; Peng, D.-L.; Zboril, R.; Varma, R. S. Core–shell nanoparticles: synthesis and applications in catalysis and electrocatalysis. *Chemical Society Reviews* **2015**, *44*, 7540–7590.

[88] Kim, H.; Achermann, M.; Balet, L. P.; Hollingsworth, J. A.; Klimov, V. I. Synthesis and characterization of Co/CdSe core/shell nanocomposites: bifunctional magnetic-optical nanocrystals. *Journal of the American Chemical Society* **2005**, *127*, 544–546.

[89] Zanella, R.; Sandoval, A.; Santiago, P.; Basiuk, V. A.; Saniger, J. M. New preparation method of gold nanoparticles on SiO2. *The Journal of Physical Chemistry B* **2006**, *110*, 8559–8565.

[90] Caruso, F.; Shi, X.; Caruso, R. A.; Susha, A. Hollow titania spheres from layered precursor deposition on sacrificial colloidal core particles. *Advanced Materials* **2001**, *13*, 740–744.

[91] Tan, S. F.; Chee, S. W.; Lin, G.; Bosman, M.; Lin, M.; Mirsaidov, U.; Nijhuis, C. A. Real-time imaging of the formation of Au–Ag core–shell nanoparticles. *Journal of the American Chemical Society* **2016**, *138*, 5190–5193.

[92] Tan, S. F.; Bisht, G.; Anand, U.; Bosman, M.; Yong, X. E.; Mirsaidov, U. In situ kinetic and thermodynamic growth control of Au–Pd core–shell nanoparticles. *Journal of the American Chemical Society* **2018**, *140*, 11680–11685.

[93] Nutt, M. O.; Hughes, J. B.; Wong, M. S. Designing Pd-on-Au bimetallic nanoparticle catalysts for trichloroethene hydrodechlorination. *Environmental Science & Technology* **2005**, *39*, 1346–1353.

[94] Zhang, N.; Liu, S.; Fu, X.; Xu, Y.-J. Synthesis of M@ TiO_2 (M= Au, Pd, Pt) core–shell nanocomposites with tunable photoreactivity. *The Journal of Physical Chemistry C* **2011**, *115*, 9136–9145.

[95] Lee, Y. W.; Kim, M.; Kim, Z. H.; Han, S. W. One-step synthesis of Au@ Pd core- shell nanooctahedron. *Journal of the American Chemical Society* **2009**, *131*, 17036–17037.

[96] Piella, J.; Bastus, N. G.; Puntes, V. Size-Controlled Synthesis of Sub-10-nanometer Citrate-Stabilized Gold Nanoparticles and Related Optical Properties. *Chemistry of Materials* **2016**, *28*, 1066–1075.

[97] Hu, J.-W.; Zhang, Y.; Li, J.-F.; Liu, Z.; Ren, B.; Sun, S.-G.; Tian, Z.-Q.; Lian, T. Synthesis of Au@ Pd core–shell nanoparticles with controllable size and their application in surface-enhanced Raman spectroscopy. *Chemical Physics Letters* **2005**, *408*, 354–359.

[98] Xia, Y.; Xia, X.; Peng, H.-C. Shape-controlled synthesis of colloidal metal nanocrystals: thermodynamic versus kinetic products. *Journal of the American Chemical Society* **2015**, *137*, 7947–7966.

[99] Li, J.; Zheng, Y.; Zeng, J.; Xia, Y. Controlling the size and morphology of Au@Pd core–shell nanocrystals by manipulating the kinetics of seeded growth. *Chemistry–A European Journal* **2012**, *18*, 8150–8156.

[100] Winey, M.; Meehl, J. B.; O'Toole, E. T.; Giddings Jr, T. H. Conventional transmission electron microscopy. *Molecular Biology of the Cell* **2014**, *25*, 319–323.

[101] Williams, D. B.; Carter, C. B. Transmission electron microscopy Plenum Press. *New York and London* **1996**.

[102] Gonon, M. Case Studies in the X-ray Diffraction of Ceramics. **2020**.

[103] Ng, L. M.; Simmons, R. Infrared spectroscopy. *Analytical Chemistry* **1999**, *71*, 343–350.

[104] Stuart, B. H., *Infrared spectroscopy: fundamentals and applications*; John Wiley & Sons: 2004.

[105] Hanrahan, P.; Krueger, W. In *Proceedings of the 20th annual conference on Computer graphics and interactive techniques*, 1993, pp 165–174.

[106] Sárkány, A.; Geszti, O.; Sáfrán, G. Preparation of Pdshell–Aucore/SiO_2 catalyst and catalytic activity for acetylene hydrogenation. *Applied Catalysis A: General* **2008**, *350*, 157–163.

[107] Laskar, M; Skrabalak, S. A balancing act: manipulating reactivity of shape-controlled metal nanocatalysts through bimetallic architecture. *Journal of Materials Chemistry A* **2016**, *4*, 6911–6918.

[108] Kariuki, V. M.; Hoffmeier, J. C.; Yazgan, I.; Sadik, O. A. Seedless synthesis and SERS characterization of multi-branched gold nanoflowers using water soluble polymers. *Nanoscale* **2017**, *9*, 8330–8340.

[109] Xie, J.; Zhang, Q.; Lee, J. Y.; Wang, D. I. The synthesis of SERS-active gold nanoflower tags for in vivo applications. *ACS Nano* **2008**, *2*, 2473–2480.

[110] Xu, J.; Wilson, A. R.; Rathmell, A. R.; Howe, J.; Chi, M.; Wiley, B. J. Synthesis and catalytic properties of Au–Pd nanoflowers. *ACS Nano* **2011**, *5*, 6119–6127.

[111] Gilroy, K. D.; Ruditskiy, A.; Peng, H.-C.; Qin, D.; Xia, Y. Bimetallic nanocrystals: syntheses, properties, and applications. *Chemical Reviews* **2016**, *116*, 10414–10472.

[112] Tessier, D.; Rakai, A.; Bozon-Verduraz, F. Spectroscopic study of the interaction of carbon monoxide with cationic and metallic palladium in palladium–alumina catalysts. *Journal of the Chemical Society, Faraday Transactions* **1992**, *88*, 741–749.

[113] Zhang, P.; Xiahou, Y.; Wang, J.; Hang, L.; Wang, D.; Xia, H. Revitalizing spherical Au@ Pd nanoparticles with controlled surface-defect density as high performance electrocatalysts. *Journal of Materials Chemistry A* **2017**, *5*, 6992–7000.

[114] Zhou, Y.; Wang, Z.; Liu, C. Perspective on CO oxidation over Pd-based catalysts. *Catalysis Science & Technology* **2015**, *5*, 69–81.

[115] Feng, C.; Liu, X.; Zhu, T.; Tian, M. Catalytic oxidation of CO on noble metal-based catalysts. *Environmental Science and Pollution Research* **2021**, 1–25.

[116] Haldar, K. K.; Kundu, S.; Patra, A. Core-size-dependent catalytic properties of bimetallic Au/Ag core–shell nanoparticles. *ACS Applied Materials & Interfaces* **2014**, *6*, 21946–21953.